First Measurement of the Proton Generalized Polarizabilities with a polarized electron beam in Virtual Compton Scattering

(VCS-IIIp)

Proposal to Jefferson Lab PAC-53

H. Atac (co-spokesperson), N. Ifat, Y. Niroula,
S. Shrestha, P. Smith, N. Sparveris (spokesperson / contact person*)
Temple University, Philadelphia, PA, USA

M. Jones (co-spokesperson)
Thomas Jefferson National Accelerator Facility, Newport News, VA, USA

M. Ali, B. Duran, M. Engelhardt,
M. Paolone (co-spokesperson), C. Paudel
New Mexico State University, NM, USA

S. Lee (co-spokesperson)
Physics Division, Argonne National Laboratory, Lemont, IL, USA

M. Kohl
Hampton University, Hampton, Virginia 23668, USA

R. Gilman
Rutgers, The State University of New Jersey, Piscataway, New Jersey 08854, USA

H. Gao, Y. Liu, B. Yu, Y. Yu, Z. Zhao, J. Zhou
Duke University, Durham, NC 27708, USA

(Dated: April 25, 2025)

* sparveri@temple.edu

Executive Summary

Main Physics Goals: The proposal focuses on the measurement of the proton electric Generalized Polarizability (GP) [61]. We propose to conduct a first measurement that follows a new experimental method, compared to the previous measurements. The experiment requires the use of a polarized beam and the measurement of beam spin asymmetries. We aim to conduct a first, independent and important cross-check to the experimental findings of the unpolarized VCS experiments and to provide unique experimental input in order to address theoretical challenges with the interpretation of the unpolarized VCS world-data.

Proposed Measurement: We propose to conduct beam spin asymmetry (BSA) measurements in the virtual Compton scattering reaction. The experiment requests to acquire data for a total of 20.5 days of beam-on-target in Hall C. If combined with the E12-23-001 (VCS-II) experiment that will run in FY-2026, 4 production days can be common for the 2 experiments. This could in-turn reduce the new beamtime request of this experiment to 16.5 days. The electric GP will be extracted from fits to the beam spin asymmetry measurements.

Specific requirements on detectors, targets, and beam: The HMS will detect protons using the standard detector package. The HMS will run at momentum between 723.7 MeV/c to 908.4 MeV/c and angles of 47° to 61°. The SHMS will detect electrons using the standard detector package. The Noble gas cerenkov detector will be removed and replaced with the existing vacuum extension. The SHMS will run at momentum 1676.4 MeV/c and angle of 17.7°. A polarized electron beam at 85% (± 3%) polarization, with energy of 2.2 GeV (± 0.2 GeV) and current of $70\mu A$ is needed for the measurements. The targets will be a 10-cm long liquid hydrogen and 10-cm aluminum dummy targets.

Previous proposals: The proposal aims to extend and strengthen the VCS experimental program at Jefferson Lab with measurements that utilize a polarized electron beam. It follows the Letter-of-Intent LOI12+23-001 (PAC51), *"Measurement of the Generalized Polarizabilities of the Proton with positron and polarized electron beams"*, and the recommendation of the PAC51 report that encourages the proponents to proceed and submit a full proposal. Here, we present a proposal for beam spin asymmetry measurements with a polarized electron beam. We leave the prospect for measurements with a positron beam to be discussed in a future proposal. Also related to the proposed experiment, the unpolarized VCS experimental program at JLab involves the following recent and upcoming experiments: E12-15-001 (VCS-I), published in [58], and experiment E12-23-001 (VCS-II) that is scheduled to acquire data in FY-2026.

.

Abstract

The electromagnetic polarizabilities are fundamental proton properties that characterize the proton's response to an external EM field. Their generalization to non-zero four-momentum transfer opens up a powerful path to study the internal structure of the proton, since they map out the spatial distribution of the polarization densities in the proton, they provide access to key dynamical mechanisms that contribute to the electric and the magnetic polarizability effects, and allow to determine fundamental characteristics of the system, such as the electric and the magnetic polarizability radii. The Generalized Polarizabilities (GPs) have so far been accessed through measurements of the virtual Compton scattering reaction, utilizing an unpolarized electron beam that is scattered from a liquid-hydrogen target. These experiments have accomplished significant advances in recent years, providing high precision benchmark data and valuable guidance to the theoretical calculations. The VCS experimental program at Jefferson Lab is active and holds a central role in the Lab's upcoming experimental schedule. Of special interest to the VCS program are theoretical challenges, in particular with regard to the interpretation of the electric polarizability measurements.

In this proposal, we follow for the first time an alternative experimental method to measure the proton GPs. The experiment utilizes a polarized electron beam for the measurement of beam spin asymmetries in virtual Compton scattering. The new measurements will offer a first, independent cross-check to the experimental findings of the unpolarized VCS experiments and will provide unique experimental input in order to address theoretical challenges with the interpretation of the world-data.

The proposal follows the Letter-of-Intent LOI12+23-001 and the recommendation of the PAC51 report that encourages the proponents to submit a full proposal, namely *"The physics case presented in the proposal is robust, and the document is very well-written. Feasibility concerns have not been identified, and the PAC encourages the proponents to proceed and submit a full proposal..."*.

I. INTRODUCTION AND MOTIVATION

A. The proton electromagnetic polarizabilities

In order to understand the underlying dynamics of quarks and gluons in the proton, as governed by quantum chromodynamics, the theoretical calculations require experimental guidance and confrontation with precise measurements of the system's fundamental properties. A wealth of information on the dynamics of the proton is hidden in the response of the proton's charge and magnetization densities to en external electromagnetic field, namely in the electromagnetic (EM) polarizabilities. The classical concept of polarizabilities was extended to the case of the nucleon with the first Compton scattering measurements on the proton in the 1950s [1–5]. A polarizability is a fundamental structure constant for any composite system, and the two scalar polarizabilities of the proton [6, 7] - the electric, α_E, and the magnetic, β_M - can be interpreted as the response of the proton's structure to an external electric or magnetic field, respectively. They describe how easily the charge and magnetization distributions inside the proton are distorted by the EM field and provide the net result on the system's spatial distributions. In order to measure the polarizabilities, one must generate an electric ($\vec{E}$) and a magnetic ($\vec{H}$) field. The electric field strength needed to induce any appreciable polarizability of the nucleon can be estimated as the ratio of the average energy level spacing in the nucleon to the size of the nucleon, namely $\approx 100\,\mathrm{MeV}/(e\,\mathrm{fm}) = 10^{23}\,\mathrm{Volt/m}$. Static electric field strengths of this intensity are not available in a laboratory. Nevertheless, in the case of the proton, this is provided by the photons in the Compton scattering process. A classical estimate of the electric field strength of a 100 MeV photon in Compton scattering from the nucleon is approximately $10^{23}\,\mathrm{Volt/m}$, allowing the Compton scattering process to be used for the experimental access of the nucleon polarizabilities.

The two scalar polarizabilities appear as second order terms in the expansion of the real Compton Scattering (RCS) amplitude in the energy of the photon

$$H^{(2)}_{eff} = -4\pi(\frac{1}{2}\alpha_E\vec{E}^2 + \frac{1}{2}\beta_M\vec{H}^2). \tag{1}$$

Considering higher orders, the 3$^{\mathrm{rd}}$-order term depends on the nucleon spin and the corresponding polarizabilities are called the *spin polarizabilities* [8]. There is no analog for them in classical electrodynamics, but they practically describe the coupling of the induced EM moments with the nucleon spin and unlike the scalar polarizabilities they are not invoked by static EM fields. Coming back to the two scalar polarizabilities, one can provide a simplistic description of these quantities based on the resulting effect of an electromagnetic perturbation applied to the nucleon constituents. An electric field moves positive and negative charges inside the proton in opposite directions. The induced electric dipole moment is proportional to the electric field, and the proportionality coefficient is the electric polarizability which quantifies the stiffness of the proton. On the other hand, a magnetic field has a different effect on the quarks and on the pion cloud within the nucleon, giving rise to two different contributions in the magnetic polarizability, a paramagnetic and a diamagnetic contribution, respectively. Compared to the atomic polarizabilities, which are of the size of the atomic volume, the proton electric polarizability α_E is much smaller than the volume scale of a nucleon [6] and the typical units adopted for the polarizabilities are $10^{-4}\,\mathrm{fm}^3$. The small magnitude underlines the stiffness of the proton, a direct consequence of the strong binding of its constituents, and indicates the intrinsic relativistic character of the system. The first Compton scattering measurement of the proton polarizabilities using a tagged photon beam was reported in [9], followed by more measurements in the next few years e.g. [10, 11]. Recent advances involve the use of linearly polarization as an analyzer to measure the electric and the magnetic polarizability independently

from each other, not relying on the Baldin sum rule [12, 13] (namely, not relying relying on the value of their sum), where the sum rule expresses the sum of dipole polarizabilities in terms of an integral of the total photoabsorption cross section σ_T:

$$\alpha_E + \beta_M = \frac{1}{2\pi^2} \int_{\nu_0}^{\infty} \nu \frac{\sigma_T(\nu)}{\nu^2} \tag{2}$$

Two experiments were reported recently. At the Mainz Microtron, Compton scattering measurements on the proton below pion threshold were performed with a tagged photon beam and a nearly 4π detector [14], and the proton polarizabilities were determined $\alpha_E = (10.99 \pm 0.16 \pm 0.47 \pm 0.17 \pm 0.34)\ 10^{-4}\ fm^3$ and $\beta_M = (3.14 \pm 0.21 \pm 0.24 \pm 0.20 \pm 0.35)\ 10^{-4}\ fm^3$, respectively. A second experiment [15] at the High Intensity Gamma-Ray Source (HIGS) facility at the Triangle Universities Nuclear Laboratory reported $\alpha_E = (13.8 \pm 1.2 \pm 0.1 \pm 0.3)\ 10^{-4}\ fm^3$ and $\beta_M = (0.2 \pm 1.2 \pm 0.1 \pm 0.3)\ 10^{-4}\ fm^3$, respectively. The tensions between the MAMI and the HIGS measurements highlights the difficulty in conducting these experiments and the need to be cautious in the treatment of the experimental uncertainties. A simultaneous extraction of the six leading-order proton polarizabilities (i.e. the two scalar and the four spin-dependent ones) using the complete set of experimental world-data was performed recently using an innovative bootstrap-base fitting method [16], leading to $\alpha_E = (12.7 \pm 0.8_{(fit)} \pm 0.1_{(model)})\ 10^{-4}\ fm^3$ and $\beta_M = (2.4 \pm 0.6_{(fit)} \pm 0.1_{(model)})\ 10^{-4}\ fm^3$.

The generalization of the two scalar polarizabilities in four-momentum transfer space [17], $\alpha_E(Q^2)$ and $\beta_M(Q^2)$, is an extension of the static electric and magnetic polarizabilities obtained in RCS. The generalized polarizabilities (GPs) are studied through measurements of the virtual Compton scattering (VCS) process [17] $\gamma^*\mathrm{p} \rightarrow \mathrm{p}\gamma$. The VCS is accessed experimentally through the $\mathrm{ep} \rightarrow \mathrm{ep}\gamma$ reaction, where the incident real photon of the RCS process is replaced by a virtual photon. The virtuality of the incident photon (Q^2) sets the scale of the observation and allows one to map out the spatial distribution of the polarization densities in the proton, while the outgoing real photon provides the EM perturbation to the system. The meaning of the GPs is analogous to that of the nucleon form factors. Their Fourier transform will map out the spatial distribution density of the polarization induced by an EM field. They probe the quark substructure of the nucleon, offering unique insight to the underlying nucleon dynamics. They allow to determine fundamental characteristics of the system, such as the EM polarizability radii, and frequently enter as input parameters in various scientific problems e.g. in the hadronic two-photon exchange corrections, which are needed for a precise extraction of the proton charge radius from muonic Hydrogen spectroscopy measurements [18].

B. Theoretical framework for the Virtual Compton Scattering

VCS at low energy and the LET: The Virtual Compton scattering (VCS) [17] reaction can be obtained from the RCS by replacing the incident real photon with a virtual photon γ^*. Experimenally the VCS can be accessed as a subprocess of the reaction $e(k) + N(p) \rightarrow e(k') + N(p') + \gamma(q')$. The particle four-momentum vectors are denoted as k^μ and k'^μ for the incoming and scattered electrons, q^μ and q'^μ for the virtual photon and final real photon, p^μ and p'^μ for the initial and final protons. The modulus of the three-momenta is denoted as $q = |\mathbf{q}|$. The variables that are indexed 'cm' are in the center-of-mass (c.m.) frame of the (initial proton + virtual photon), namely the c.m. of the Compton process. The kinematics of the reaction are defined by five independent variables. The set of variables that is typically adopted involves $(q_{cm}, q', \epsilon, \theta_{cm}, \phi)$, where ϵ is the virtual photon

polarization parameter, i.e.,

$$\epsilon = 1/[1 + 2\frac{q^2_{\rm lab}}{Q^2}\tan^2(\theta'_{e\,\rm lab}/2)]. \tag{3}$$

The q_{cm} and q' are the three-momentum modulus of the virtual photon and final photon in the c.m., respectively, θ_{cm} and ϕ are the c.m. angles of the Compton process, namely the polar and azimuthal angles of the outgoing real photon w.r.t. the virtual photon. In the above reaction, the real final photon can be emitted by either the electron or the nucleon. The first contribution corresponds to the Bethe-Heitler (BH) process, which is well known and calculable from QED with the nucleon electromagnetic form factors as an input. The second part involves the VCS subprocess. The VCS can in-turn be decomposed further to a Born term, where the intermediate state is a nucleon, and a non-Born term which contains all nucleon excitations and meson-loop contributions. The non-Born amplitude $T^{\rm NB}$ contains the physics of interest and is parametrized at low energy by the nucleon GPs. The three amplitudes add up coherently to form the total photon electroproduction amplitude, namely

$$T^{ep\to ep\gamma} \;=\; T^{BH} \;+\; T^{Born} \;+\; T^{NB} \;=\; T^{BH} \;+\; T^{VCS}\,. \tag{4}$$

In obtaining the non-Born amplitude, a multipole expansion [28] is performed in the c.m. frame, yielding the multipoles $H^{(\rho' L',\rho L)S}_{\rm NB}(q'_{cm}, q_{cm})$. Here $L\,(L')$ represents the angular momentum of the initial (final) electromagnetic transition in the $(\gamma^* p \to \gamma p)$ process, and S differentiates between the spin-flip $(S = 1)$ or non spin-flip $(S = 0)$ transition at the nucleon side. $[\rho\,(\rho') = 0, 1, 2]$ characterizes the longitudinal (L), electric (E) or magnetic (M) nature of the initial (final) photon. The GPs are obtained as the limit of these multipoles when q'_{cm} tends to zero, at arbitrary fixed q_{cm}. At this strict threshold the final photon has zero frequency, its electric and magnetic fields are constant, corresponding to a "static field", and the GPs represent the generalization at finite q_{cm} of the polarizability in classical electromagnetism. For small values of q'_{cm} one may use the dipole approximation $(L' = 1)$, corresponding to electric and magnetic final-state radiation that is dipolar only. In this case, angular momentum and parity conservation lead to ten different dipole GPs [28], that the nucleon crossing combined with charge conjugation symmetry then reduces further to six independent GPs [25, 39], namely the two scalar GPs $(S = 0)$ and the four spin-dependent (or spin-flip) GPs $(S = 1)$. The two scalar GPs, the electric and magnetic, are thus defined as:

$$\alpha_E(Q^2) = -\frac{e^2}{4\pi}\cdot\sqrt{\frac{3}{2}}\cdot P^{(L1,L1)0}(Q^2) \tag{5}$$

$$\beta_M(Q^2) = -\frac{e^2}{4\pi}\cdot\sqrt{\frac{3}{8}}\cdot P^{(M1,M1)0}(Q^2) \tag{6}$$

with $e^2/4\pi = \alpha_{QED} = 1/137$ and at $Q^2 = 0$ they coincide with the RCS static electromagnetic polarizabilities α_E and β_M.

At low energy q' of the emitted photons, the low-energy theorem (LET) and the low-energy expansion (LEX) for VCS [28] state that the non-Born term starts at order q' whereas the Born term enters at $1/q'$. They offer a model-independent approach which allows to express the VCS cross section in terms of the GPs and to access GPs through experiments via the $ep \to ep\gamma$ reaction. The LEX formula yields for the photon electroproduction cross section below the pion production threshold:

$$d\sigma = d\sigma_{BH+Born} + \Phi q'_{cm}\,\Psi_0 + \mathcal{O}(q'^2_{\rm cm}) \tag{7}$$

$$\Psi_0 = V_1\,(P_{LL} - P_{TT}/\epsilon) + V_2\,P_{LT}, \tag{8}$$

Here $d\sigma_{BH+Born}$ is the BH+Born cross section, that is entirely calculable in QED and requires the nucleon elastic form factors G_E and G_M as an input. It contains no polarizability effect and serves as an important cross section of reference throughout the whole formalism. The $(\Phi q'_{cm})$, V_1 and V_2 are kinematical factors. The term $(\Phi q'_{cm}\,\Psi_0)$ is where the GPs first appear in the expansion. Ψ_0 is the first-order polarizability term, obtained from the interference between the BH+Born and non-Born amplitudes at the lowest order. It is therefore of order $q'^0_{\rm c.m.}$, namely independent of $q'_{\rm cm}$. In the phase-space factor $(\Phi q'_{cm})$, the term q'_{cm} has been explicitly factored out in order to emphasize the fact that when q'_{cm} tends to zero, the $(\Phi q'_{cm}\,\Psi_0)$ tends to zero and the whole cross section tends to $d\sigma_{BH+Born}$. The $\mathcal{O}(q'^2_{\rm cm})$ term represents all the higher-order terms of the expansion and contains GPs of all orders. Below the pion production threshold, $d\sigma_{BH+Born}$ dominates the cross section, Ψ_0 is the leading polarizability term and the higher-order terms $\mathcal{O}(q'^2_{\rm cm})$ are expected to be negligible. The Ψ_0 term contains three VCS response functions, or structure functions: P_{LL}, P_{LT}, and P_{TT}, which are combinations of the lowest-order GPs

$$P_{LL}(Q^2) = -2\sqrt{6}M_N \cdot G_E^p(Q^2) \cdot P^{(L1,L1)0}(Q^2) \tag{9}$$

$$P_{TT}(Q^2) = -3G_M^p(Q^2) \cdot \frac{q_{cm}^2}{\tilde{q}^0} \cdot \left(P^{(M1,M1)1}(Q^2) - \sqrt{2}\tilde{q}^0 \cdot P^{(L1,M2)1}(Q^2) \right) \tag{10}$$

$$P_{LT}(Q^2) = \sqrt{\frac{3}{2}} \cdot \frac{M_N \cdot q_{cm}}{\tilde{Q}} \cdot G_E^p(Q^2) \cdot P^{(M1,M1)0}(Q^2) + \left[\frac{3}{2} \frac{q_{cm}\sqrt{Q^2}}{\tilde{q}^0} \cdot G_M^p(Q^2) \cdot P^{(L1,L1)1}(Q^2) \right] \tag{11}$$

where M_N is the mass of the nucleon. Here we can point out that P_{LL} is proportional to the electric GP, P_{LT} has a spin-independent part that is proportional to the magnetic GP, plus a spin-dependent part $P_{LT\,spin}$, and P_{TT} is a combination of two spin GPs.

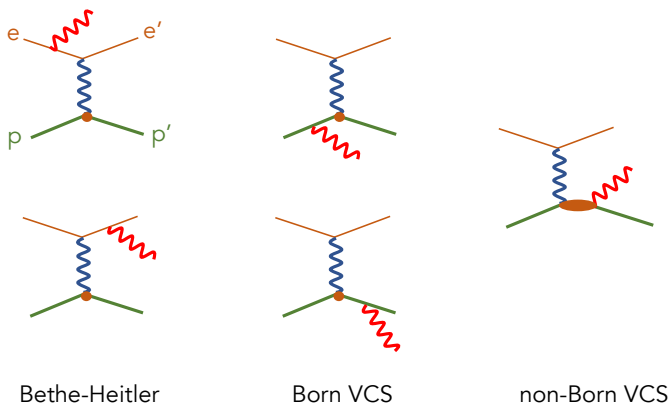

FIG. 1: Feynman diagrams of photon electroproduction. The small circles represent the interaction vertex of a virtual photon with a proton considered as a point-like particle, while the ellipse denotes the non-Born VCS amplitude.

The Dispersion Relation formalism: The LEX of the VCS observables provides a model independent method to analyze VCS experiments below pion-production threshold in terms of structure functions which contain information on GPs. Nevertheless, the sensitivity of the VCS cross section to the GPs is enhanced in the region between pion-production threshold and the Δ-resonance region,

where the LEX does not hold. Here the dispersive approach provides a valuable theoretical framework to extract the GPs. In the DR formalism, the non-Born contribution to the VCS scattering amplitude is parametrized in terms of twelve independent amplitudes $F_i(Q^2, \nu, t)$, $i = 1, \ldots, 12$, which depend on three kinematical invariants, Q^2, t, and the crossing-symmetric variable $\nu = (s-u)/(4M_N)$ [26]. The GPs are expressed in terms of the non-Born part F_i^{NB} at the point $t = -Q^2$ and $\nu = 0$. Assuming an appropriate analytic and high-energy behavior, these amplitudes fulfil unsubtracted DRs in the variable ν at fixed t and fixed Q^2:

$$\mathrm{Re}\, F_i^{NB}(Q^2, \nu, t) = F_i^{pole}(Q^2, \nu, t) - F_i^{B}(Q^2, \nu, t) + \frac{2}{\pi}\mathcal{P}\int_{\nu_{thr}}^{+\infty} \mathrm{d}\nu' \frac{\nu' \mathrm{Im}\, F_i(Q^2, \nu', t)}{\nu'^2 - \nu^2}, \tag{12}$$

where F_i^B is the Born contribution as defined in [28, 29], whereas F_i^{pole} denote the nucleon pole contributions. Furthermore, $\mathrm{Im}\, F_i$ are the discontinuities across the s-channel cuts, starting at the pion production threshold $\nu_{thr} = m_\pi + (m_\pi^2 + t/2 + Q^2/2)/(2M)$. The validity of the unsubtracted DRs in Eq. 12 relies on the assumption that at high energies ($\nu \to \infty$, fixed t and fixed Q^2) the amplitudes drop fast enough such that the integrals converge. The high-energy behavior of the amplitudes F_i was investigated in [26, 27], with the finding that the integrals diverge for F_1 and F_5. For energies up to the Δ-resonance region, one can saturate the s-channel dispersion integral by the πN contribution, setting the upper limit of integration to $\nu_{max} = 1.5$ GeV. The remainder can be estimated by energy-independent functions, which parametrize the asymptotic contribution due to t-channel poles, as well as the residual dispersive contributions beyond the value $\nu_{max} = 1.5$ GeV. The asymptotic contribution to F_5 is saturated by the π^0 pole [26]. The asymptotic contribution to F_1 can be described phenomenologically as the exchange of an effective σ meson, in the same spirit as for unsubtracted DRs in the RCS case. The Q^2 dependence of this term is unknown. It can be parametrized in terms of a function directly related to the magnetic dipole GP $\beta_M(Q^2)$ and fitted to VCS observables. Furthermore, it was found that the unsubtracted DR for the amplitude F_2 is not so well saturated by πN intermediate states only. The additional s-channel contributions beyond the πN states can effectively be accounted for with an energy-independent function, at fixed Q^2 and $t = -Q^2$. This amounts to introducing an additional fit function, which is directly related to the electric dipole GP $\alpha_E(Q^2)$. In order to provide predictions for VCS observables, it is convenient to adopt the following parametrizations for the fit functions:

$$\alpha_E(Q^2) - \alpha_E^{\pi N}(Q^2) = \frac{\alpha_E^{exp} - \alpha_E^{\pi N}}{(1 + Q^2/\Lambda_\alpha^2)^2}, \quad \beta_M(Q^2) - \beta_M^{\pi N}(Q^2) = \frac{\beta_M^{exp} - \beta_M^{\pi N}}{(1 + Q^2/\Lambda_\beta^2)^2}, \tag{13}$$

where α_E and β_M are the RCS polarizabilities, with superscripts exp and πN indicating, respectively, the experimental value and the πN contribution evaluated from unsubtracted DRs. In Eq. 13, the mass scale parameters Λ_α and Λ_β are free parameters, not necessarily constant with Q^2, which can be adjusted by a fit to the experimental cross sections.

The LEX and DR frameworks have illustrated a remarkable agreement and consistency in their extracted values of the scalar GPs from all the reported experiments. Data below the pion production threshold were analyzed and compared with both the LEX and the DR. Moreover, the polarizabilities were extracted via VCS measurements that were conducted above the pion threshold, utilizing the DR formalism, and the results were in excellent agreement with the results from the measurements below the pion production threshold. One fundamental difference between the two (LEX vs DR) analysis methods is that the DR formalism allows for a direct extraction of the scalar GPs, by fitting the parameters Λ_α and Λ_β to the data. The LEX analysis on the other hand gives access to structure functions that depend linearly on both scalar and spin GPs [28]. In order to disentangle the scalar GPs, the contribution from the spin GPs to the structure functions has to be subtracted using a model, and for that one typically uses the DR prediction for the spin GPs.

C. Theoretical calculations of the generalized polarizabilities

Theoretical calculations for the Virtual Compton Scattering have been performed within a a variety of frameworks. The first calculations were based on the non relativistic constituent quark model (NRCQM) [28, 30, 31]. It was later extended [32] to include relativistic effects by considering a Lorentz covariant multipole expansion of the VCS amplitude and a light-front relativistic calculation of the nucleon excitations. The constituent quark model calculations have limitations, but have been constructive e.g. in providing a first approximate estimate for the nucleon resonance contributions to the GPs. The resonance contribution to the GPs has been accounted for more accurately within the effective lagrangian model (ELM). These calculations are based on a fully relativistic effective Lagrangian framework, which includes baryon resonance contributions as well as π^0 and σ exchanges in the t-channel [33, 34], or on calculations that use a coupled-channel unitary approach [35]. Calculations within the framework of the linear sigma model (LSM) and chiral effective field theories offer a different perspective through the prism of chiral symmetry and the pionic degrees of freedom. The LSM allows for a simplistic description of the nucleon that is based on the relevant symmetries like Lorentz, gauge and chiral invariance. These calculations [36, 37] revealed the existence of relations between the VCS multipoles, in addition to the usual constraints of parity and angular momentum conservation [38, 39]. The contribution of the pion-cloud effects can be accounted for using chiral perturbation theories (ChPTs), an expansion in the external momenta and the pion mass ("p"-expansion). The VCS amplitude comes consistent with electromagnetic gauge invariance, the pattern of chiral symmetry breaking in QCD, and Lorentz covariance, to a given order of the small parameter $p \equiv \{P, m_\pi\}/\Lambda$, where P stands for each component of the four-momenta of the photons and of the three-momenta of the nucleons and Λ is the breakdown scale of the theory. The first calculation [40, 41] was performed at $\mathcal{O}(p^3)$ with only nucleons and pions as explicit degrees of freedom, using the heavy-baryon (HB) expansion for the nucleon propagators, which amounts to making an expansion in $1/M_N$ along with the expansion in p. The calculations were later on extended to to $\mathcal{O}(p^4)$ and to $\mathcal{O}(p^5)$ [42, 43]. The inclusion of the $\Delta(1232)$ as an explicit degree of freedom in the calculation of the VCS process was first accounted for in [44], by introducing the excitation energy of the $\Delta(1232)$ as an additional expansion parameter ("ϵ expansion"). An alternative counting has also been proposed in [45] ("δ-expansion") and it was employed for the VCS process in [46] using a manifestly Lorentz invariant version of baryon chiral perturbation theory (BChPT).

In Fig. 2 a representative group of the above calculations is shown. The differences in the Q^2 dependence of the calculations can be traced to a number of parameters. In the NRCQM the excited states of the nucleon are given by resonances, and the Q^2 behavior of the GPs is determined by the electromagnetic transition form factors, the LSM accounts for the excitation spectrum as pion-nucleon scattering states with a different Q^2 dependence and predicts a rapid variation at small momentum transfer and a smooth one at higher momentum, while the ELM allows for both resonant and non-resonant contributions. A common feature of all the calculations is that they underestimate the static electric polarizability at the real photon point by $\sim 30\%$. For the magnetic GP, the pion cloud contributes to a positive slope at the origin, while the $N \to \Delta$ transition form factor drives the paramagnetic contribution, which decreases as function of Q^2. The LSM describes only the negative diamagnetic component, the NRCQM accounts only for the positive paramagnetic contribution, while the interplay of the two competing effects can be observed in the ELM calculation. The calculation at next-to-leading order in baryon chiral perturbation theory (BChPT) [46] is also shown in Fig. 2. Here, the consideration of the pion-cloud effects allows to overcome the shortcomings of the previous models in accounting for the magnitude of the static electric polarizability. The BChPT prediction comes with a sizable theoretical uncertainty of $\sim 30\%$ that pointing to the need for the

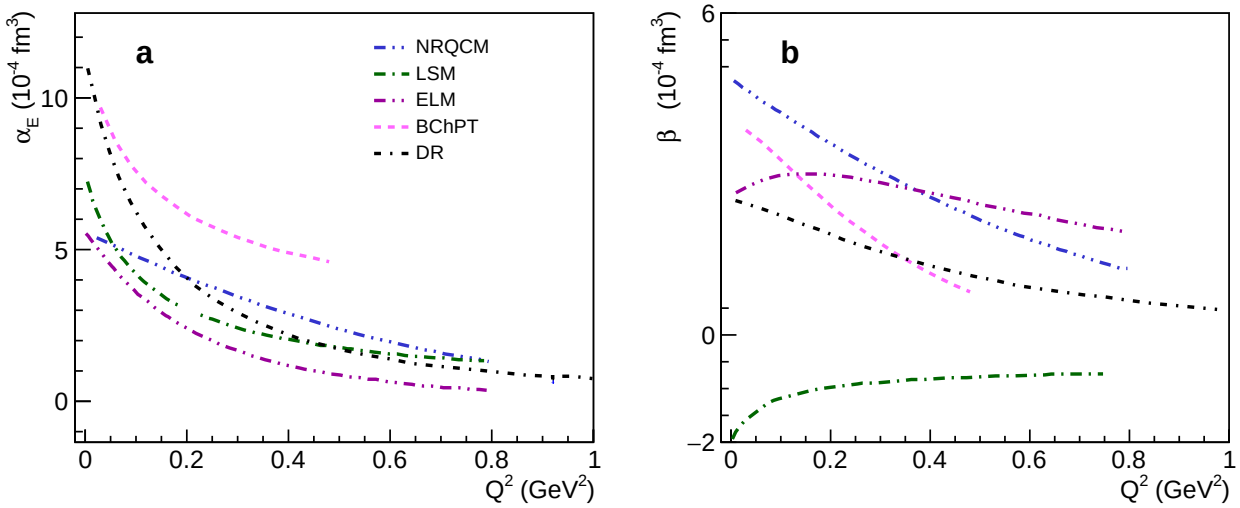

FIG. 2: The theoretical predictions of BChPT [46], NRQCM [31], LSM [36], ELM [35] and DR [21, 26, 27] are shown for the electric generalized polarizability (left) and for the magnetic generalized polarizability (right).

next order calculation.

D. Experimental measurements of the generalized polarizabilities

The VCS experimental measurements span a period of three decades, with the first one taking place in 1995 [47, 48]. The experiments were conducted at MAMI, MIT-Bates and JLab, following a similar technique, namely utilizing an unpolarized electron beam, a liquid hydrogen target, and the detection of the two charged particles e' and p' in magnetic spectrometers. The exclusive reaction is identified using the missing mass squared of the undetected photon, and the extraction of GPs from the VCS cross section measurements is conducted via a fit through either the LEX or the Despersion Relations framework.

The first measurements (MAMI-I experiment) [47, 48] made use of the A1 experimental setup at MAMI. The experiment was pioneering since it was the first to establish and implement all the experimental considerations of the VCS measurements, from the design of the experiment to the numerous aspects of the data analysis e.g. the radiative corrections, dedicated Monte-Carlo simulations, the implementation of the LEX fit methods for the GP extraction, etc. The measurements targeted the region below the pion-production threshold, covering an extended range in photon energies, but were limited to in-plane angles. The first experiment at JLab [49, 50] explored the highest photon virtualities so far, in the range $Q^2 = 1 - 2\ GeV^2$. The GPs were found to be very small, pointing to a rapid fall-off with Q^2. For a common Q^2, data were taken both below and above the pion-production threshold, and the extraction of the GPs was done independently for the two data sets. This allowed to show for the first time that the GP extractions both below and above the pion production threshold, using respectively the LEX and DR formalisms, gave consistent results. It was also shown that the sensitivity to the polarizabilities is amplified when one measures above the pion threshold and into the nucleon resonance region. The MIT-Bates experiment [51, 52] was the first to use extracted CW beam from the MIT-Bates South Hall Ring and it exploited the potential of the out-of-plane kinematics. It took advantage of the unique strengths of the Out-of-Plane Spectrometer (OOPS) system, namely to access large out-of-plane angles, combined with the ability to perform simultaneous measurements at different azimuthal angles, using up to four identical, lightweight

magnetic spectrometers. This offered a significant reduction to the systematic uncertainties of the measurement. Data were taken at the smallest Q^2 so far (namely at 0.057 GeV^2), allowing the first extraction of the mean-square electric polarizability radius of the proton. This experiment was also the first one to evidence a bias in the LEX fit and to highlight the limitations in using this method of extraction for the GPs. An exploratory measurement of beam spin asymmetries was also conducted at MAMI [111] but these results exhibited a very weak sensitivity to the polarizabilities as shown in in Fig. 3.

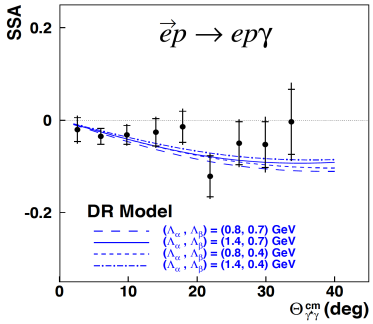

FIG. 3: Figure from reference [111]. The beam SSA in photon electroproduction at $Q^2 = 0.35\ GeV^2$ is compared to the calculation of the DR model for several values of the free parameters Λ_α and Λ_β. The inner error bar is statistical, the outer one is the quadratic sum of statistical and systematic errors.

This group of early experiments shaped a preliminary understanding of the proton electric and magnetic GPs, covering a broad range in momentum-transfer. The measurements came with relatively large experimental uncertainties, in particular for the magnetic polarizability, highlighting the experimental challenges in extracting the weak magnetic polarizability signal. One puzzling observation of the reported measurements involved the electric GP. Here the data pointed out an enhancement of the α_E magnitude at $Q^2 = 0.33$ GeV^2, compared to the other measurements, that violates the theoretical expectation for a monotonic fall-off as a function of Q^2. Consequently, a follow-up experiment was conducted at MAMI, at the same $Q^2 = 0.33$ GeV^2, aiming to provide a cross-check and confirm the findings of the MAMI-I. The measurements of the MAMI-IV experiment [53] used the same experimental setup and focused on angular kinematics very similar to MAMI-I, and confirmed the results that were previously reported by MAMI-I.

The experiments that followed in recent years focused on providing a finer Q^2 mapping of the polarizabilities and on improving the precision of the results. A central part of the attention focused on understanding the puzzling structure of $\alpha_E(Q^2)$ that was confirmed by two independent experiments. The MAMI-V experiment [54] determined the electric GP at $Q^2 = 0.20$ GeV^2 from cross section and asymmetry measurements in the $\Delta(1232)$ resonance. Here, the α_E extraction was performed exclusively within the DR framework, since the LEX formalism is not applicable in the $\Delta(1232)$ region. In parallel to the polarizability measurement, the experiment offered the first extraction of the $N \to \Delta$ quadrupole amplitude through the photon excitation channel. The MAMI-VI experiment [55] explored three values of $Q^2 = 0.10$, 0.20 and 0.45 GeV^2. The structure functions and the scalar GPs were extracted with a high precision from cross-section data below the pion production threshold, utilizing both the LEX and the DR formalism. Out-of-plane kinematics were selected at each Q^2, in line with the approach of the MIT-Bates experiment, but they covered a larger angular phase space. Capitalizing on the experience acquired from the previous measurements, a novel bin selection method was developed aiming to suppress the higher-order terms of the LEX. The DR model was utilized to provide an estimate of the higher-order terms of the LEX expansion. The

theoretical cross sections, $d\sigma_{\rm DR}$ and $d\sigma_{\rm LEX}$, were calculated using the same input values of structure functions. Since $d\sigma_{\rm DR}$ includes all orders in $q'_{c.m.}$, the difference $(d\sigma_{\rm DR} - d\sigma_{\rm LEX})$ is a measure of the higher-order terms $\mathcal{O}(q'^2_{\rm c.m.})$ of Eq. 7, as given by the DR model. Accordingly, the following dimensionless estimator was constructed:

$$\mathcal{O}(q'^2_{\rm c.m.})_{DR} = \frac{d\sigma_{\rm DR} - d\sigma_{\rm LEX}}{d\sigma_{\rm BH+Born}} \tag{14}$$

at each point in the VCS phase space. The model-dependent estimator was used first in the design of the experiment in order to define kinematics where $\mathcal{O}(q'^2_{\rm c.m.})$ is expected to be small. It was later on employed in the data analysis of the experiment to study the behavior of the LEX fit under varying conditions. LEX fits were performed including a varying number of experimental bins, corresponding to gradually increased values of the $\mathcal{O}(q'^2_{\rm c.m.})_{DR}$ estimator by setting the condition $\mathcal{O}(q'^2_{\rm c.m.})_{DR} \leq K$ and letting the threshold K vary. Polarizability LEX fits were performed and their results were compared with and without the novel bin selection method, while a comparison was also done with the results of the DR fit analysis that is not bound to similar restrictions in the phase space selection. The analysis indicated that the effect of the higher-order contributions becomes small and less of a concern at momentum transfers higher than 0.4 GeV^2, while careful consideration should be given in the data analysis at lower momentum transfers so that these effects get eliminated via an appropriate phase-space masking. The refinements in the MAMI-VI data analysis allowed to eliminate any bias arising from the higher-order contributions and minimized the systematic uncertainties in the extraction of the GPs. This refined analysis procedure was afterwards utilized for a reanalysis [56] of the MAMI-I and MAMI-IV data. Compared to the results of the original analysis, the extracted values for the α_E were mildly reduced, but the change was not considerable to eliminate the observed structure in the electric GP.

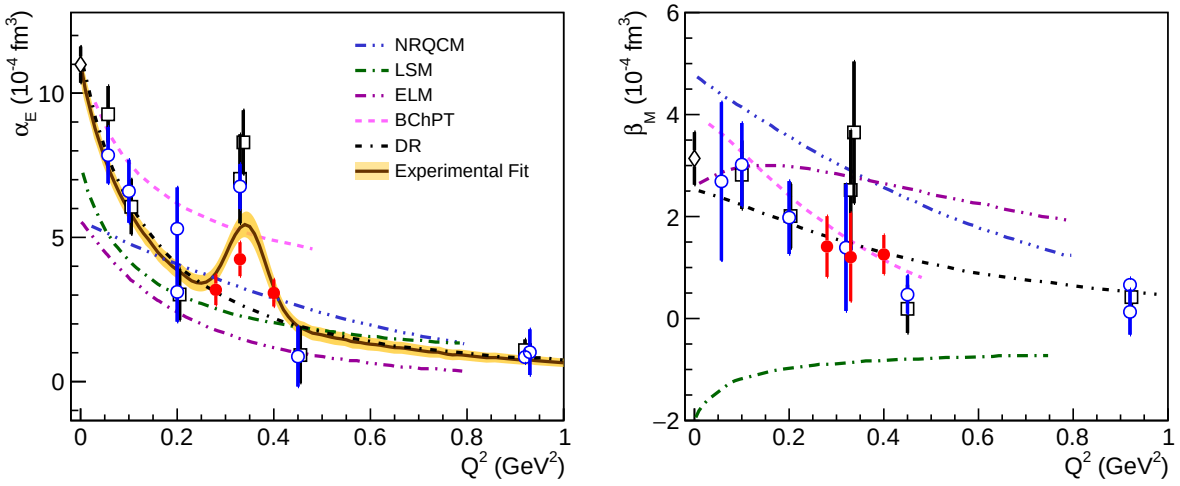

FIG. 4: The electric and the magnetic generalized polarizability measurements. The VCS-I results [57] are shown as red-circles and the world data [14, 47–49, 51, 53–55] as open-symbols. The results from the Dispersion-Relation fits and the Low-Energy-Expansion fits are shown as circles and boxes, respectively. The theoretical predictions of BChPT [46], NRQCM [31], LSM [36], ELM [35] and DR [21, 26, 27] are also shown.

The most recent measurements involve the VCS program in Hall C at Jefferson Lab. The first phase of this program, namely the VCS-I experiment [57], acquired data in 2019 focusing on precision measurements within the region (Q^2=0.28 GeV^2-0.40 GeV^2) where the puzzling structure of $\alpha_E(Q^2)$ has been reported. Electrons with energies of 4.56 GeV at a beam current up to 20 μA were produced by Jefferson Lab's Continuous Electron Beam Accelerator Facility and were scattered from a 10 cm

long liquid-hydrogen target. The Super High Momentum Spectrometer (SHMS) and the High Momentum Spectrometer (HMS) of Hall C were used to detect in coincidence the scattered electrons and recoil protons, respectively. Cross section measurements were conducted for azimuthally symmetric kinematics in the photon angle, namely for $(\phi_{\gamma^*\gamma}, \pi - \phi_{\gamma^*\gamma})$, since the measurement of the azimuthal asymmetry in the cross section enhances the sensitivity in the extraction of the polarizabilities and suppresses part of the systematic uncertainties. Moreover, the ep→epπ^0 reaction was measured, simultaneously with the ep→epγ reaction. The pion electroproduction cross section is well known in this kinematic regime, and it's measurement offered a stringent, real-time normalization control to the measurement of the ep→epγ cross section. Overall, the VCS-I experiment accomplished a significant improvement in the precision of the extracted generalized polarizabilities compared to the previous measurements. The extracted GPs from the VCS-I experiment are shown in Fig. 4. The measurements suggest a local enhancement of $\alpha_E(Q^2)$ in the measured region, at the same Q^2 as previously reported in [47, 48, 53], but with a smaller magnitude than what was originally suggested. The Q^2-dependence of the electric GP was explored using two types of approaches [57], namely methods that employ traditional fits to the data using predefined functional forms, as well as methods that are based on data-driven techniques that assume no direct underlying functional form. Both methods point to a Q^2-dependence for $\alpha_E(Q^2)$ that is consistent with the presence of a structure in the measured region, in sharp contrast with the current theoretical understanding that suggests a monotonic dependence of $\alpha_E(Q^2)$ with Q^2. For $\beta_M(Q^2)$, the results point to a smooth Q^2-dependence and the near-cancellation of the paramagnetic and the diamagnetic contributions in the proton at $\sim Q^2$=0.4 GeV^2. A comparison with the theory predictions of BChPT [46], NRQCM [31], LSM [36], ELM [35] and DR [21, 26, 27] is shown in Fig. 4. The theoretical predictions for the GPs vary noticeably, and the experimental results impose strict constraints to the theory.

The VCS program at JLab will continue with the VCS-II experiment (E12-23-001) [58]. The measurements will employ the SHMS-HMS spectrometers, an unpolarized electron beam (at $E_\circ = 1.1\ GeV$ and $2.2\ GeV$) and a 10 cm liquid-hydrogen target. The first part of the VCS-II is scheduled to run from February to July, 2026. The measurements will extend the kinematic coverage of the measured GPs while providing high precision data combined with a fine Q^2 mapping, from $Q^2 = 0.05\ (GeV/c)^2$ to $Q^2 = 0.50\ (GeV/c)^2$, as shown in Fig. 5. The measurements will be of unprecedented precision as well as uniform in regard to their systematic uncertainties. This will make possible to identify the shape of the observed structure in the electric polarizability precisely and reliably. Moreover, the precision of the β_M measurements will be further improved to allow a good handle on the interplay between the diamagnetic and paramagnetic contributions in the nucleon.

E. Induced polarization in the proton and polarizability radii

The generalized polarizabilities allow to generate a tomographic profile of the polarizability effect in the proton, and provide access to the spatial deformation of the quark distributions subject to the influence of an electromagnetic field [59]. For that, one follows a method that is an extension of the formalism to extract the light-front quark charge densities from the proton form factor data. An extraction of the induced polarization in the proton from the experimental measurements has been carried out in [57]. An accurate parametrization of the polarizabilities was derived from a fit to the experimental data. From that, the induced polarization in the proton, P_0, is extracted following the formalism in [59], namely

$$\vec{P}_0(\vec{b}) = \hat{b} \int_0^\infty \frac{dQ}{(2\pi)}\, Q\, J_1(b\,Q)\, A(Q^2), \tag{15}$$

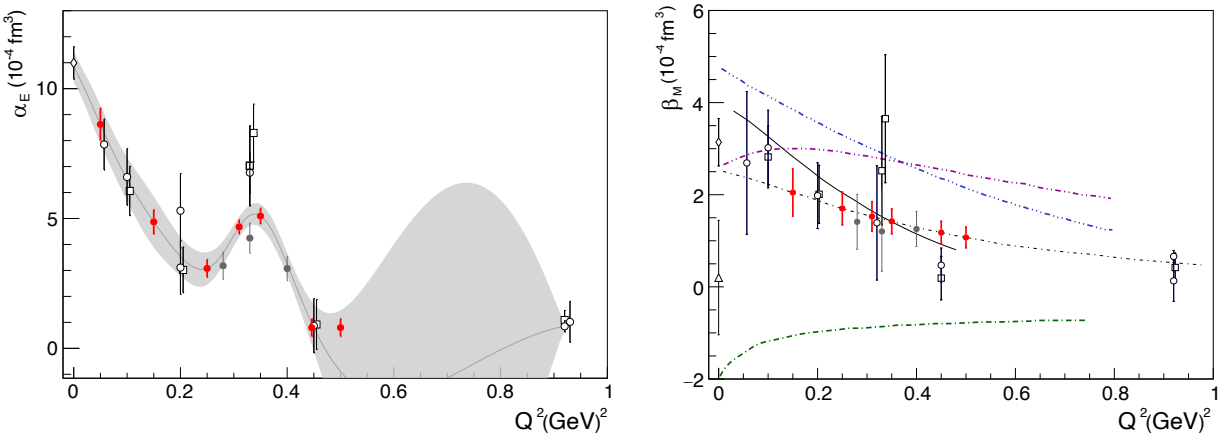

FIG. 5: The VCS-II projected measurements for α_E and β_M are shown as red solid points. The world data are shown with open symbols, with the exception of the VCS-I results that are indicated with filled gray circles. The gray-band in the electric GP plot indicates the data-driven extraction of the polarizability from [57].

where $\vec{b}$ is the transverse position, $b = |\vec{b}|$, $\hat{b} = \vec{b}/b$ and J_1 the 1st order Bessel function. The A is a function of the GPs :

$$A = -(2M_N)\sqrt{\tau}\sqrt{\frac{3}{2}}\sqrt{\frac{1+2\tau}{1+\tau}}$$
$$\times\left\{-P^{(L1,L1)0} + \frac{1}{2}P^{(M1,M1)0} - \sqrt{\frac{3}{2}}P^{(L1,L1)1}\right.$$
$$\left.-\sqrt{\frac{3}{2}}(1+\tau)\left[P^{(M1,M1)1} + \sqrt{2}\,(2M_N\tau)P^{(L1,M2)1}\right]\right\}. \quad (16)$$

The GPs are expressed in the typical multipole notation $P^{(\rho'\,l',\rho\,l)S}$ [28], where ρ (ρ') refers to the Coulomb/electric (L), or magnetic (M) nature of the initial (final) photon, l ($l' = 1$) is the angular momentum of the initial (final) photon, and S differentiates between the spin-flip ($S = 1$) and non spin-flip ($S = 0$) transition at the nucleon side. The $\tau \equiv Q^2/(4M_N^2)$, with M_N the nucleon mass. In calculating the A function, the two scalar GPs are defined through Eq. 5 and Eq. 6 and the spin GPs are fixed by the dispersion relations. For the asymptotic part of $\alpha_E(Q^2)$, an experimental fit to the world-data leads to the following parametrization [57]:

$$\alpha_E(Q^2) = \left[p0 * e^{-0.5*(\frac{Q^2-p1}{p2})^2} + \frac{1}{(p3 + Q^2/p4)^2}\right] \ (fm^3) \quad (17)$$

The $\beta_M(Q^2)$ world data follow a single dipole behavior with a mass scale parameter of $\Lambda_\beta = 0.5\ GeV$ and are described accurately by the DR model [21, 26, 27]. The derived induced polarization as a function of the transverse position in the proton is shown in Fig. **??**. The distribution follows a change of sign around ∼0.25 fm and exhibits a secondary maximum in the amplitude around ∼0.35 fm.

The primary measure to quantify the spatial extension of the polarizability effect is provided by the mean square polarizability radii. The mean square electric polarizability radius of the proton $\langle r^2_{\alpha_E}\rangle$ can be determined from the VCS measurements, as it is related to the slope of the $\alpha_E(Q^2)$ at $Q^2 = 0$ by

$$\langle r^2_{\alpha_E}\rangle = \frac{-6}{\alpha_E(0)} \cdot \frac{d}{dQ^2}\alpha_E(Q^2)\Big|_{Q^2=0}. \quad (18)$$

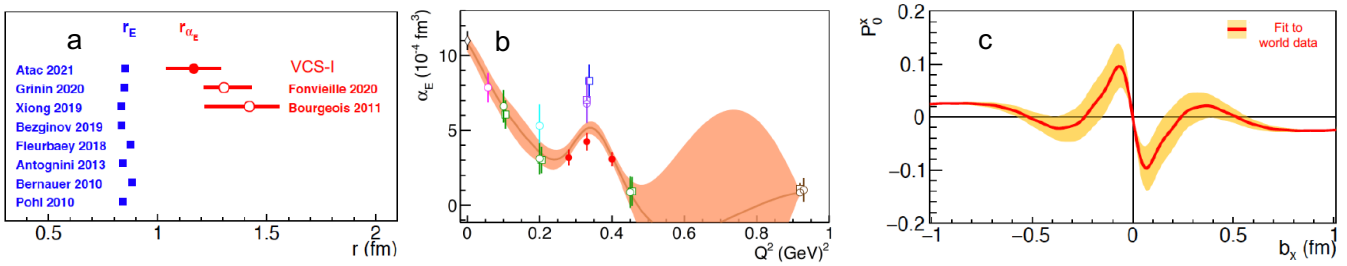

FIG. 6: **a)** The proton electric polarizability radius $r_{\alpha_E} \equiv \sqrt{\langle r^2_{\alpha_E}\rangle}$ is shown in red. The measurements of the proton charge radius are shown for comparison in blue color. **b)** The Q^2-dependence of the electric GP as derived from the experimental measurements using the GPR technique [106], a data-driven method that assumes no direct underlying functional form. **c)** Induced polarization in the proton when submitted to an EM field as a function of the transverse position with photon polarization along the x axis for $b_y = 0$. The x-y defines the transverse plane, with the z axis being the direction of the fast moving protons.

A first $\langle r^2_{\alpha_E}\rangle$ extraction became possible with the MIT-Bates measurements at $Q^2 = 0.057\ GeV^2$ [51]. It was determined from a dipole fit to the RCS and the MIT-Bates data points, giving $\langle r^2_{\alpha_E}\rangle = 1.95 \pm 0.33\ fm^2$ [51]. Since then, a more accurate extraction has been conducted [57], taking into account a complete data-set from the modern experiments in tandem with a comprehensive consideration of the fitted functional forms and of the fitting range. The analysis employed a variety of functional forms that can fit the data (i.e. combinations of polynomial, dipole, gaussian, exponential functions). The fits were considered in two groups: one that fitted the full Q^2 range, and a second one that focused on a limited range at low-Q^2 (i.e. excluding the α_E anomaly), namely within Q^2=[0,0.28] GeV^2. For the polarizabilities derived by both the Dispersion Relations and the Low Energy Expansion analysis, the variance of the two results is treated as a model uncertainty for each data point. For each group of fits, the final value for $\langle r^2_{\alpha_E}\rangle$ is determined from the weighted average of the results of the individual fits. The uncertainty of $\langle r^2_{\alpha_E}\rangle$ receives contributions from two terms, the uncertainty of the weighted average and from the weighted variance of the individual fit results, that effectively reflects the model dependence on the choice of the fitted parametrization. The final result is then derived from the average of the two group values, with their spread accounted as a model uncertainty. The extraction of the polarizability radius is sensitive to the value of the static ($Q^2 = 0$) electric polarizability. For example, if one considers the recent measurement from MAMI [14], $\alpha_E(0) = (10.99 \pm 0.16 \pm 0.47 \pm 0.17 \pm 0.34)\ 10^{-4}\ fm^3$, the extracted value for the polarizability radius is $\langle r^2_{\alpha_E}\rangle = 1.36 \pm 0.29\ fm^2$ (we note that the MAMI measurement [14] is in excellent agreement with the PDG value for $\alpha_E(0)$). A recent experiment at HIGS [15] illustrates tension to the MAMI measurement (albeit with a high experimental uncertainty) and reports a higher value of $\alpha_E(0) = (13.8 \pm 1.2 \pm 0.1 \pm 0.3)\ 10^{-4}\ fm^3$. Addopting the HIGS value for $\alpha_E(0)$, one derives $\langle r^2_{\alpha_E}\rangle = 1.67 \pm 0.50\ fm^2$. In both cases, the extracted $\langle r^2_{\alpha_E}\rangle$ is considerably larger compared to the mean square charge radius of the proton, namely $\langle r^2_E\rangle \sim 0.7\ fm^2$ [6, 60]. The dominant contribution to this effect is expected to arise from the deformation of the mesonic cloud in the proton under the influence of an external EM field.

For the extraction of the mean square magnetic polarizability radius from the magnetic polarizability measurements, one follows a procedure that is equivalent to the extraction of the $\langle r^2_{\alpha_E}\rangle$ since the magnetic polarizability radius expression is similar, namely

$$\langle r^2_{\beta_M}\rangle = \frac{-6}{\beta_M(0)} \cdot \frac{d}{dQ^2}\beta_M(Q^2)\Big|_{Q^2=0} \tag{19}$$

and from a fit to the world-data one can derive $\langle r^2_{\beta_M}\rangle = 0.63 \pm 0.31\ fm^2$.

II. EXPERIMENTAL DETAILS OF THE PROPOSED MEASUREMENTS

A. Proposed VCS Beam Spin Asymmetry Measurements and Required Equipment

One challenge with the polarizability world-data is that they suggest a non-trivial α_E dependence, that deviates at the 3σ level from the theory prediction of a monotonic Q^2 fall-off. This observation presents a striking contradiction to the current theoretical understanding of this fundamental proton property. The signature of the effect has been explored [62] with phenomenological fits and with data-driven methods e.g. as shown in Fig. 6(b). More measurements are needed to exclude the possibility that this observation is coincidental. That being the case, the shape and the dynamical signature of this structure needs to be mapped with precision, so that it can serve as an input for the theory in order to explain the effect. Considering the alternative scenario, a monotonic fall-off for the electric polarizability would testify that there is a strong tension among the experimental world data. This would in-turn suggest that when analyzing the virtual Compton scattering measurements, there are currently processes or sources of systematic uncertainty that get routinely underestimated and are not yet well understood.

The experimental study of the proton generalized polarizabilities has so far employed just one method, namely the measurement of absolute cross sections in VCS using unpolarized electron beams. The VCS-II at JLab will be the next experiment of this series of measurements. It will acquire data in FY-2026 and will provide the most comprehensive study of the GPs in terms of precision via unpolarized VCS measurements. Nevertheless, in parallel to the unpolarized VCS measurements, it is critical to employ an alternative experimental method that has the capacity to offer an independent confirmation of the experimental findings. This can be particularly valuable in regard to confirming and understanding the observed structure in the electric polarizability. Employing alternative experimental methods for the measurement of a physics signal is a key element in the scientific process. The scientific merit of cross-checking physics measurements by contradicting alternative experimental methods and comparing their results, has been illustrated on several occasions in the past. One we can briefly refer to a couple of examples here e.g. the measurement of the proton elastic form factors (Rosenbluth vs recoil polarization) and the measurement of the proton charge radius (scattering vs spectroscopy). In both cases, the application of orthogonal methods to measure a physics quantity has proven instrumental in advancing the scientific process.

The use of polarized and positron beams provides an alternative and powerful avenue to access the proton GPs. The lepton beam charge (e) and polarization (λ) dependence of the $lp \to lp\gamma$ differential cross section is given by

$$d\sigma^e_\lambda = d\sigma_{\rm BH} + d\sigma_{\rm VCS} + \lambda\, d\tilde{\sigma}_{\rm VCS} + e\,(d\sigma_{\rm INT} + \lambda\, d\tilde{\sigma}_{\rm INT}), \tag{20}$$

where $d\sigma$ ($d\tilde{\sigma}$) are the polarization independent (dependent) contributions which are even (odd) functions of the azimuthal angle ϕ. The $d\sigma_{\rm INT}$ involves the real part of the VCS amplitude that contains the GP effects, while $d\tilde{\sigma}_{\rm INT}$ is proportional to the imaginary part of the VCS amplitude which does not depend on the GPs. Combining lepton beams of opposite charge and different polarization enables the complete separation of the four unknown INT and VCS contributions. More specifically, using unpolarized electron and positron beams, one can construct the unpolarized beam-charge asymmetry (BCA) A^C_{UU} as

$$A^C_{UU} \;=\; \frac{(d\sigma^+_+ + d\sigma^+_-) - (d\sigma^-_+ + d\sigma^-_-)}{d\sigma^+_+ + d\sigma^+_- + d\sigma^-_+ + d\sigma^-_-}$$

$$= \frac{d\sigma_{\rm INT}}{d\sigma_{\rm BH} + d\sigma_{\rm VCS}}. \tag{21}$$

With polarized lepton beams, on the other hand, one can construct the lepton beam-spin asymmetry (BSA)

$$\begin{aligned} A^e_{LU} &= \frac{d\sigma^e_+ - d\sigma^e_-}{d\sigma^e_+ + d\sigma^e_-} \\ &= \frac{d\tilde{\sigma}_{\rm VCS} + e d\tilde{\sigma}_{\rm INT}}{d\sigma_{\rm BH} + d\sigma_{\rm VCS} + e\, d\sigma_{\rm INT}}. \end{aligned} \tag{22}$$

The theoretical groundwork and a first theoretical exploration for the potential of this type of measurements has been conducted in [112]. These studies illustrated that the un-polarized BCA asymmetries and the polarized BSA asymmetries exhibit remarkable sensitivity to both scalar GPs. A combination of both types of assymmetries, such as

$$\begin{aligned} \tilde{A}_{\rm VCS} &\equiv A^+_{LU}\left(1 + A^C_{UU}\right) + A^-_{LU}\left(1 - A^C_{UU}\right) \\ &= \frac{2d\tilde{\sigma}_{\rm VCS}}{d\sigma_{\rm BH} + d\sigma_{\rm VCS}}, \end{aligned} \tag{23}$$

and

$$\begin{aligned} \tilde{A}_{\rm INT} &\equiv A^+_{LU}\left(1 + A^C_{UU}\right) - A^-_{LU}\left(1 - A^C_{UU}\right) \\ &= \frac{2d\tilde{\sigma}_{\rm INT}}{d\sigma_{\rm BH} + d\sigma_{\rm VCS}} \end{aligned} \tag{24}$$

is powerful towards separating the contribution from the $d\tilde{\sigma}_{\rm VCS}$ and $d\tilde{\sigma}_{\rm INT}$ terms, offering both sensitivity to the GPs as well as a cross-check of the unitarity input in the dispersive formalism, as discussed in [112].

In this proposal, we capitalize on [112], we continue the work in the Letter-of-Intent LOI12+23-001, and follow the PAC51 report recommendation to propose the first measurement of GPs that is based on this new method using the experimental apparatus that is readily available at Jefferson Lab.

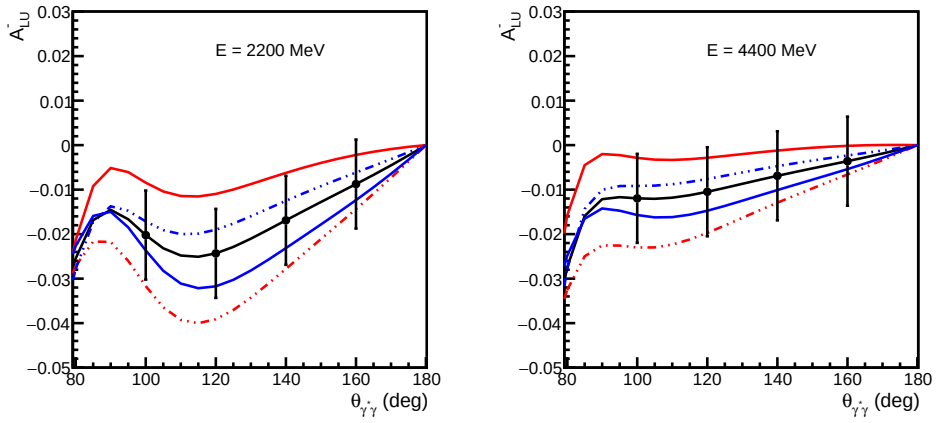

FIG. 7: Sensitivity of the BSA measurements to the GPs for two different beam energies of E=2.2 GeV and 4.4 GeV, respectively, for a common subset of the projected data in the measured phase-space. The black curve corresponds to mass scale parameters Λ_α=Λ_β=0.7. The two red (blue) curves explore the sensitivity to the electric (magnetic) GP by varying the Λ_α (Λ_β) from 0.5 to 0.9.

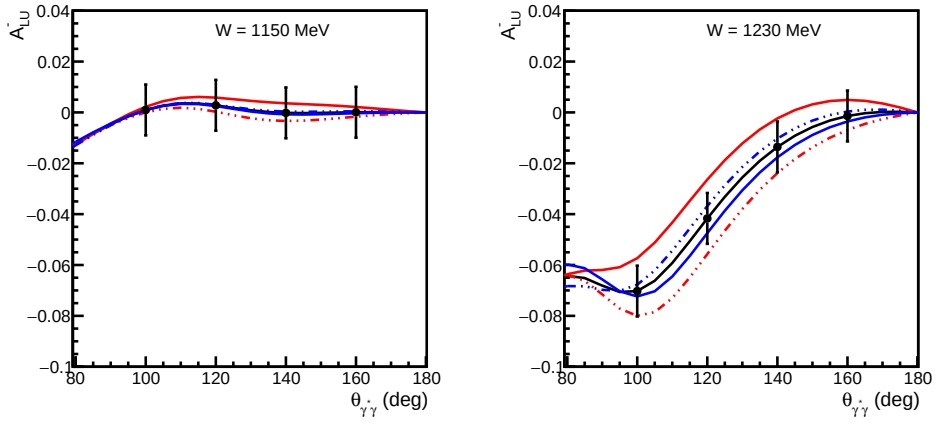

FIG. 8: Sensitivity of the BSA measurements to the GPs at the lower wing vs the top of the Δ resonance.

More specifically, we propose using a polarized electron beam to measure the beam spin asymmetries (BSA) in VCS. These measurements can be best accommodated in Hall C, using the SHMS and the HMS experimental setup. **For the proposed measurements, the SHMS and the HMS spectrometers will be utilized in their standard configuration (namely, as they will be used during the VCS-II (E12-23-001) experiment). The only additional requirement, compared to the VCS-II experiment, is that of a polarized electron beam.** Our goal is to perform a first precise measurement of $\alpha_E(Q^2)$ through the beam spin asymmetries, compare it to the corresponding $\alpha_E(Q^2)$ extraction from the unpolarized VCS experiments, and provide an independent confirmation of the findings that have been reported for the electric polarizability. Towards that end, the central kinematics of the experiment have been selected at $Q^2 = 0.35\ GeV^2$. This is where the experimental fits, using either predefined functional forms or data-driven analysis methods, predict a maximum in the observed structure. Extensive simulation studies have been performed in order to determine the key parameters of the experimental measurements and for the study of systematic uncertainties. A series of studies focused on the determination of the optimal beam energy for the experiment, as shown e.g. in Fig. 7. The vicinity of a $E = 2\ GeV$ beam energy offers the best sensitivity to the polarizabilities. The sensitivity to the polarizabilities also varies with the center of mass energy. The studies showed a weak sensitivity at the lower wing of the Δ resonance, that gradually grows on the top and above the peak of the resonance, as shown e.g. in Fig. 8. The experiment kinematics have been optimized accordingly to cover the range of $W = 1190\ MeV$ to $W = 1280\ MeV$. In terms of the photon angle, the studies show that one has to stay above $\theta_{\gamma^*\gamma} = 100°$. Coincidently, part of the kinematics of interest for the proposed experiment overlaps with some kinematics of the VCS-II (E12-23-001) experiment that is currently scheduled to acquire data in spring 2026. As such, we give care in matching the corresponding kinematics of the current proposal to that of the VCS-II experiment. A benefit here is that a part of the VCS-II measurements, that will run next year, could collect in-parallel and for free a fraction of the data for the BCA measurements, provided that the beam during the VCS-II will be polarized. In such a case, the beam-time request of this proposal can be reduced by 4 production days.

The beam-spin-asymmetry allows to suppress several systematic uncertainties, that one would otherwise deal with in an absolute cross section measurement. Several parameters that contribute to the BSA systematic uncertainties have been investigated with a series of simulation studies, in which the simulation has been weighted with the Disperson Relations model for VCS [21, 26, 27], as shown e.g. in Fig. 9 and Fig. 10. The acceptance and bin-migration effects contribute $\sim 5\%$ to the

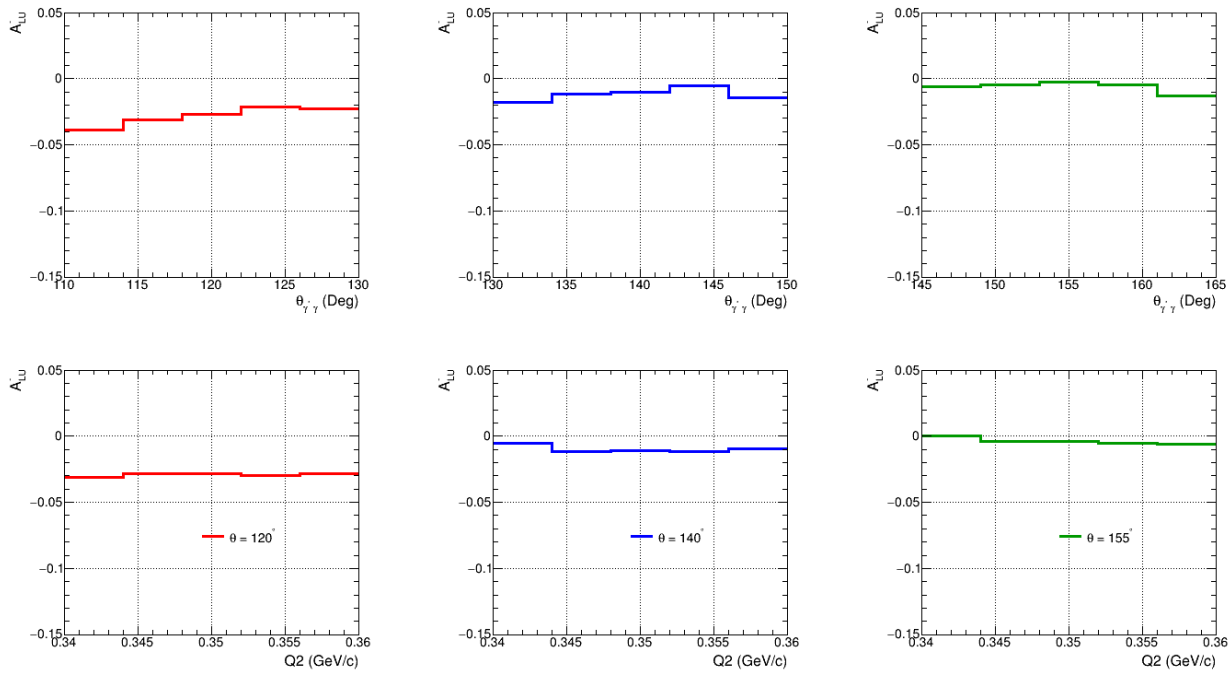

FIG. 9: Simulation of three experiment settings (from left to right $\theta_{\gamma^*\gamma} = 120^\circ, 140^\circ, 155^\circ$). The beam spin asymmetry within the phase space is shown vs $\theta_{\gamma^*\gamma}$ (top) and Q^2 (bottom), respectively.

systematic uncertainty, with a small variance across the different settings. The uncertainty due to the bin-centering correction varies from $\sim 6\%$ to 8%. The systematic uncertainties due to the background subtraction, to the dummy (target wall) subtraction, and to the pion contamination are much smaller, at $\sim 1\%$ or less each. The systematic uncertainty due to radiative effects is $\sim 2\%$ to 3% and that of the beam polarization is 3%. The overall effect of the systematic uncertainties to the measurement is considerably smaller compared to the projected statistical uncertainty (typically $\sim 50\%$ of the statistical), thus rendering the statistics the limiting factor of the proposed measurements.

B. Kinematics and Beamtime Request

The kinematic settings for the proposed measurements are listed in Table I. The HMS singles rates will be $\sim$ a few tens kHz, the SHMS singles rates will be $\sim$250 kHz, and the coincidence signal to noise (S/N) ratio will be $\sim$5. The measured phase space will be binned and the beam spin asymmetries will be measured over a wide range of center-of-mass energies and photon angles, for $Q^2 = 0.35\ GeV^2$. The generalized electric polarizability will then be extracted through a DR fit [21, 26, 27] to the data set of the beam spin asymmetries. Considering that the measurement is statistics limited, we have explored two scenaria with respect to the beam-time request. The first one involves an ideal scenario in terms of statistics, that represents the formal beamtime request of the proposal. As shown in Table I, it involves 20 days of production beamtime. An additional 0.5 days is requested for dummy target runs and various check outs, thus bringing the total beamtime request to 20.5 days. Here we note that 4 days of this beamtime can be shared with the VCS-II experiment, which will acquire data in spring 2026, provided that the beam will be polarized. We have communicated this prospect to the lab and have been informed that there is no limitation with the lab providing a polarized beam during these measurements, so that it will benefit both

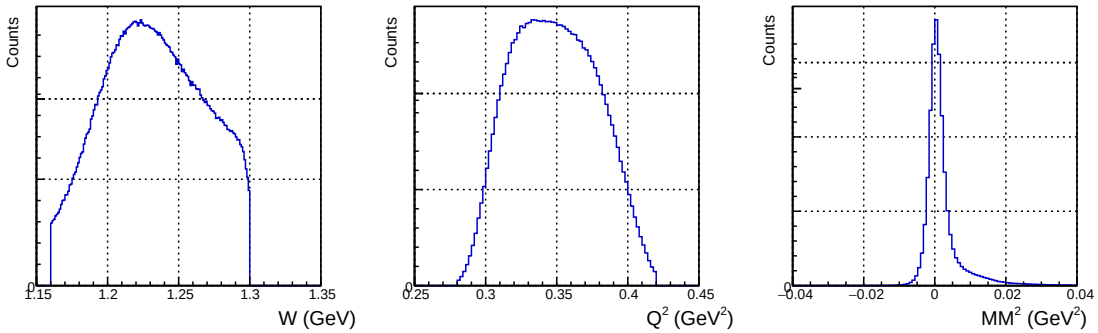

FIG. 10: Simulation of the experiment showing the center of mass energy, Q^2 and the reconstructed missing mass spectrum for one kinematic setting.

experiments. That being the case, the request for new beamtime gets reduced to 16.5 days. The projected measurement for the electric GP is shown in Fig. 11.

Beam Energy (GeV)	Beam Current (uA)	Beam Requirements	Target	θ_e°	$P_e^{'}$ (MeV/c)	θ_p°	$P_p^{'}$ (MeV/c)	Beamtime (days)
2.2	70	Polarized	LH2 (10cm)	17.72	1676.41	60.71	723.69	2 (1.5)
2.2	70	Polarized	LH2 (10cm)	17.72	1676.41	56.21	808.93	6 (3.5)
2.2	70	Polarized	LH2 (10cm)	17.72	1676.41	51.12	874.74	6 (3.5)
2.2	70	Polarized	LH2 (10cm)	17.72	1676.41	47.10	908.37	6 (4)
Total Time								20 (12.5)

TABLE I: The beamtime request per kinematic setting for the production data taking. The alternative scenario of reduced beamtime, as discussed in the document, is given in the parenthesis.

In parallel, we have explored the impact of a second, more economic scenario in terms of beamtime. We consider that the PAC will find this useful in making an informed decision considering that run

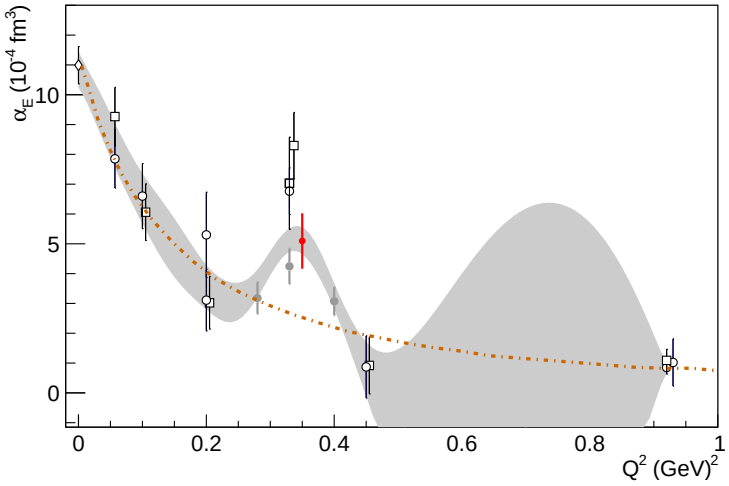

FIG. 11: The projected measurement for the proposed experiment. The projected measurement for the α_E from the BSA measurements is shown in red, along with the world data. The data-driven extraction of α_E is shown with the gray band [57] and the α_E dipole dependence is plotted with the dash-dot curve.

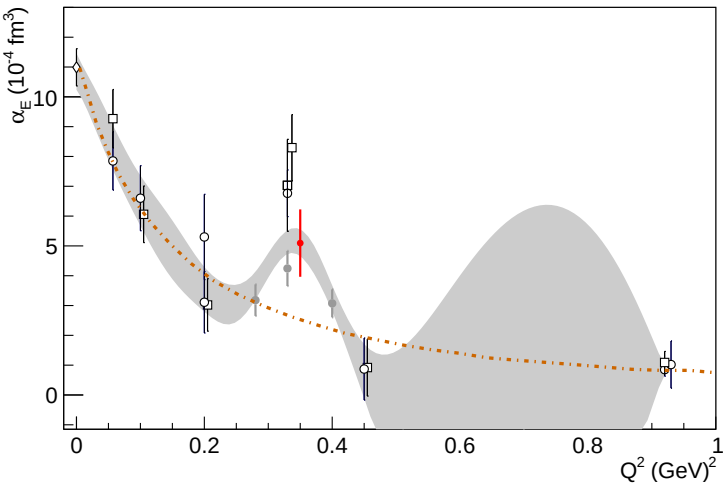

FIG. 12: The projected measurement for the α_E from the BSA measurements, based on the more economic beamtime scenario, is shown in red along with the world data.

time is a valuable and scarce resource. The production beamtime in this scenario comes down to 12.5 days, as shown in the parenthesis of Table I. Adding another 0.5 day for dummy runs and check outs brings up the beamtime to a total of 13 days. Similarly to above, if this combines with the VCS-II data taking, the overall beamtime request can be reduced to a total of 9 days of beam on target. The projected measurement for this scenario is shown in Fig. 12. As shown in the figure, while the uncertainty of the measurement increases by 20% a very competitive $\alpha_E(Q^2)$ extraction can still be accomplished within this more economic beamtime scenario.

C. Prospects with a positron beam

For the completeness of the physics discussion, we briefly discuss the future prospects in conducting polarizability measurements utilizing a positron beam. Nevertheless, we do not include any beamtime request for this component in the proposal, considering that a positron beam is currently not available at JLab, and will not be available in the near future. The goal here is to provide to the reader with a complete overview on future prospects with potential measurements using positrons. There are two type of measurements that once can pursue here. One potential path involves the measurement of the unpolarized beam-charge asymmetry with a combination of electron and positron beams. Our studies have targeted one momentum transfer setting at $Q^2 = 0.35\ GeV^2$ and involve a beam energy of $E_\circ = 2.2\ GeV$. With the SHMS and the HMS measuring $e^{(+,-)}$ and p respectively, we have focused within a range of center of mass energies that exhibits good sensitivity to the polarizabilities, spanning $W = 1150\ MeV$ to $W = 1190\ MeV$. Here, it becomes beneficial to measure out of plane kinematics and the experimental setup offers access at $\phi = 30^o$. We have considered a kinematic range of measurements in $\theta_{\gamma^*\gamma}$ that spans a range as e.g. shown in Fig. 13 for one bin in W. We have considered a scenario of measurements that allows enough statistics so as to bring the statistical uncertainty for each of the (+,-) measurements to the 1%. Here, the uncertainty of the results is already limited by systematic uncertainties. The projected α_E measurement for this set of kinematics is shown at the right panel of Fig. 13. An equally competitive extraction to the magnetic GP is also projected by these measurements. The group of kinematics with an electron beam requires 1 week of beamtime, with a beam current of $I \sim 50\ \mu A$, depending on the kinematics.

The kinematic group counterpart with the positron beam will require more beamtime, since the beam current will be smaller in this case. The exact beamtime will depend on the final performance of the delivered positron beam. The unpolarized positron beam is expected at the level of $\sim \mu A$ level. With an optimistic scenario that one can achieve 5 μA, about 10 weeks of beamtime would be required in such a case for a measurement as shown in Fig. 13. A note can be made here, that since these projections involve measurements that are systematics limited, one could also cut-down the beam-on-target time to some extent, aiming to balance a more economic beam-time request while not inflating significantly the projected uncertainty in the extraction of the polarizability. Our preliminary studies presented here illustrate a superb potential for accessing the physics of interest through measurements that will employ an unpolarized positron beam and we intend to follow up on this work with a series of complete and comprehensive studies.

We have also considered the measurement of BSA with a positron beam. For a group of similar measurements (namely, at the same kinematics and of the same precision, as in the case of the electron beam measurements) the sensitivity in the extraction of the polarizabilities is equaly competitive (and slightly better) compared to the measurements with an electron beam. Nevertheless, the issue here involves the beamtime that is needed for such measurements, since the beam current for a polarized positron beam will be significantly suppressed. For example, if one considers an average beam current of $I \sim 50\ nA$ and a beam polarization of 60%, one is facing the need of a beamtime that is 3 orders of magnitude higher compared to the measurements with an electron beam. We consider that this path is not viable, based on the expected performance of a future positron beam at JLab.

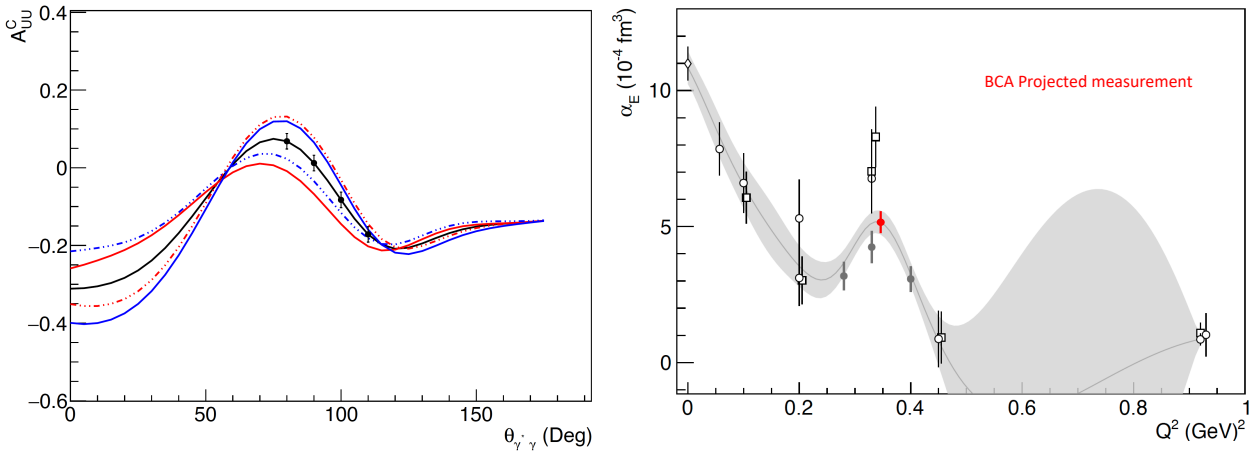

FIG. 13: Beam charge asymmetry measurements with a positron and an electron beam. Left panel: measurements at a fixed bin at $W = 1170\ MeV$ and $\phi = 30^o$. The black curve corresponds to mass scale parameters Λ_α=Λ_β=0.7. The two red (blue) curves explore the sensitivity to the electric (magnetic) GP by varying the Λ_α (Λ_β) from 0.5 to 0.9. Right panel: the projected measurement for the α_E from the BCA measurements is shown in red, along with the world data.

III. SUMMARY

In this proposal, we discuss a new method for the measurement of the proton generalized polarizabilities. We propose to conduct a first measurement of the electric generalized polarizability using a polarized electron beam and measuring beam spin asymmetries in virtual Compton scattering. The proposed measurements will offer for the first time an independent cross check to the findings

of the unpolarized VCS experiments and will provide unique experimental data that are needed in addressing theoretical challenges with the interpretation of the world data. Employing alternative experimental methods for the measurement of a physics signal is a key element in the scientific process. The proposed experiment comes to enrich and strengthen an ongoing research program at Jefferson Lab by providing a unique measurement. It will allow to improve our understanding of a fundamental proton property, thus advancing our understanding of the nucleon structure.

The experiment will make use of the SHMS and HMS spectrometers in Hall C, in their standard configuration. A polarized electron beam at 85% (± 3%) polarization, with energy of 2.2 GeV (± 0.2 GeV) and current of 70μA is needed for the measurements, along with the 10-cm long liquid hydrogen and 10-cm aluminum dummy targets. The beamtime request for the measurements is 20.5 days. We note that if the proposed measurements are conducted in tandem with the scheduled VCS-II experiment, the two experiments can share 4 days of common beamtime, thus reducing the new beamtime request of this proposal to 16.5 days.

---

[1] Oxley CL, Telegdi VL. Scattering of 30- to 95-mev photons by protons. Phys Rev (1955) 100:435–6. doi:10.1103/PhysRev.100.435

[2] Oxley CL. Scattering of 25-87 Mev photons by protons. Phys Rev (1958) 110:733–7. doi:10.1103/PhysRev.110.733

[3] Pugh GE, Gomez R, Frisch DH, Janes GS. Nuclear scattering of 50- to 130-mev gamma rays. Phys Rev (1957) 105:982–95. doi:10.1103/PhysRev.105.982

[4] Hyman LG, Ely R, Frisch DH, Wahlig MA. Scattering of 50- to 140-mev photons by protons and deuterons. Phys Rev Lett (1959) 3:93–6. doi:10.1103/PhysRevLett.3.93

[5] Bernardini G, Hanson AO, Odian AC, Yamagata T, Auerbach LB, Filosofo I. Proton compton effect. Nuovo Cim (1960) 18:1203–36. doi:10.1007/BF02733177

[6] Zyla PA, Barnett RM, Beringer J, Dahl O, Dwyer DA, Groom DE, et al. Review of particle physics. PTEP 2020 (2020) 2020:083C01. doi:10.1093/ptep/ptaa104

[7] Downie EJ, Fonvieille H. Real and virtual compton scattering: the nucleon polarisabilities. Eur Phys J ST (2011) 198:287–306. doi:10.1140/epjst/e2011-01495-x

[8] Ragusa S. Third order spin polarizabilities of the nucleon. Phys Rev D (1993) 47: 3757–67. doi:10.1103/PhysRevD.47.3757

[9] Federspiel FJ, Eisenstein RA, Lucas MA, MacGibbon BE, Mellendorf K, Nathan AM, et al. The Proton Compton effect: a Measurement of the electric and magnetic polarizabilities of the proton. Phys Rev Lett (1991) 67:1511–4. doi:10.1103/PhysRevLett. 67.1511

[10] Blanpied G, Blecher M, Caracappa A, Deininger R, Djalali C, Giordano G, et al. N —¿ delta transition and proton polarizabilities from measurements of p (gamma polarized, gamma), p (gamma polarized, pi0), and p (gamma polarized, pi+). Phys Rev C (2001) 64:025203. doi:10.1103/PhysRevC.64.025203

[11] de León VO, Wissmann F, Achenbach P, Ahrens J, Arends HJ, Beck R, et al. Low-energy Compton scattering and the polarizabilities of the proton. Eur Phys J (2001) 10:207–15. doi:10.1007/s100500170132

[12] Baldin A. Polarizability of nucleons. Nucl Phys (1960) 18:310–7. doi:10.1016/0029-5582(60)90408-9

[13] Lapidus L. Scattering of gamma quanta and polarizability of nuclei and nucleons. Sov Phys JETP (1963) 16:964.

[14] Mornacchi E, Martel P, Abt S, Achenbach P, Adlarson P, Afzal F, et al. Measurement of compton scattering at mami for the extraction of the electric and magnetic polarizabilities of the proton. Phys Rev Lett (2022) 128:132503. doi:10.1103/PhysRevLett.128.132503

[15] Li X, Ahmed M, Banu A, Bartram C, Crowe B, Downie E, et al. Proton compton scattering from linearly polarized gamma rays. Phys Rev Lett (2022) 128:132502. doi:10. 1103/PhysRevLett.128.132502

[16] Mornacchi E, Rodini S, Pasquini B, Pedroni P. First concurrent extraction of the leading-order scalar and spin proton polarizabilities. Phys Rev Lett (2022) 129:102501. doi:10.1103/PhysRevLett.129.102501

[17] Fonvieille H, Pasquini B, Sparveris N. Virtual compton scattering and nucleon generalized polarizabilities. Prog Part Nucl Phys (2020) 113:103754. doi:10.1016/j.ppnp. 2020.103754

[18] Pasquini B, Vanderhaeghen M. Dispersion theory in electromagnetic interactions. Ann Rev Nucl Part Sci (2018) 68:75–103. doi:10.1146/annurev-nucl-101917-020843

[19] Hagelstein F, Miskimen R, Pascalutsa V. Nucleon polarizabilities: from compton scattering to hydrogen atom. Prog Part Nucl Phys (2016) 88:29–97. doi:10.1016/j.ppnp. 2015.12.001

[20] Guichon PAM, Vanderhaeghen M. Virtual Compton scattering off the nucleon. Prog Part Nucl Phys (1998) 41:125–90. doi:10.1016/S0146-6410(98)00056-8

[21] Drechsel D, Pasquini B, Vanderhaeghen M. Dispersion relations in real and virtual Compton scattering. Phys Rept (2003) 378:99–205. doi:10.1016/S0370-1573(02)00636-1

[22] Griesshammer HW, McGovern JA, Phillips DR, Feldman G. Using effective field theory to analyse low-energy Compton scattering data from protons and light nuclei. Prog Part Nucl Phys (2012) 67:841–97. doi:10.1016/j.ppnp.2012.04.003
[23] Holstein BR, Scherer S. Hadron polarizabilities. Ann Rev Nucl Part Sci (2014) 64:51–81. doi:10.1146/annurev-nucl-102313-025555
[24] Geng L. Recent developments in SU(3) covariant baryon chiral perturbation theory. Front Phys (Beijing) (2013) 8:328–48. doi:10.1007/s11467-013-0327-7
[25] Drechsel D, Knochlein G, Korchin AY, Metz A, Scherer S. Low-energy and low momentum representation of the virtual Compton scattering amplitude. Phys Rev (1998) C58:1751–7. doi:10.1103/PhysRevC.58.1751
[26] Pasquini B, Gorchtein M, Drechsel D, Metz A, Vanderhaeghen M. Dispersion relation formalism for virtual Compton scattering off the proton. Eur Phys J (2001) A11: 185–208. doi:10.1007/s100500170084
[27] Pasquini B, Drechsel D, Gorchtein M, Metz A, Vanderhaeghen M. Dispersion relation formalism for virtual Compton scattering and the generalized polarizabilities of the nucleon. Phys Rev (2000) C62:052201. doi:10.1103/PhysRevC.62.052201
[28] Guichon PAM, Liu GQ, Thomas AW. Virtual Compton scattering and generalized polarizabilities of the proton. Nucl Phys (1995) A591:606–38. doi:10. 1016/0375-9474(95)00217-O
[29] Guichon PAM, Vanderhaeghen M. Virtual Compton scattering off the nucleon. Prog Part Nucl Phys (1998) 41:125–90. doi:10.1016/S0146-6410(98)00056-8
[30] Liu GQ, Thomas AW, Guichon PAM. Virtual Compton scattering from the proton and the properties of nucleon excited states. Austral J Phys (1996) 49:905–18. doi:10.1071/PH960905
[31] Pasquini B, Scherer S, Drechsel D. Generalized polarizabilities of the proton in a constituent quark model revisited. Phys Rev (2001) C63:025205. doi:10.1103/PhysRevC. 63.025205
[32] Pasquini B, Salmè G. Nucleon generalized polarizabilities within a relativistic constituent quark model. Phys Rev (1998) C57:2589–96. doi:10.1103/PhysRevC.57.2589
[33] Vanderhaeghen M. Virtual Compton scattering study below pion production threshold. Phys Lett (1996) B368:13–9. doi:10.1016/0370-2693(95)01495-0
[34] Vanderhaeghen M. Double polarization observables in virtual Compton scattering. Phys Lett (1997) B402:243–50. doi:10.1016/S0370-2693(97)00500-5
[35] Korchin AY, Scholten O. Nucleon polarizabilities in virtual Compton scattering. Phys Rev (1998) C58:1098–100. doi:10.1103/PhysRevC.58.1098
[36] Metz A, Drechsel D. Generalized polarizabilities of the nucleon studied in the linear sigma model. Z Phys (1996) A356:351–7. doi:10.1007/s002180050188
[37] Metz A, Drechsel D. Generalized polarizabilities of the nucleon studied in the linear sigma model. 2. Z Phys (1997) A359:165–72. doi:10.1007/s002180050384
[38] Drechsel D, Knochlein G, Korchin AY, Metz A, Scherer S. Structure analysis of the virtual Compton scattering amplitude at low-energies. Phys Rev (1998) C57:941–52. doi:10.1103/PhysRevC.57.941
[39] Drechsel D, Knochlein G, Metz A, Scherer S. Generalized polarizabilities and the spin averaged amplitude in virtual Compton scattering off the nucleon. Phys Rev (1997) C55:424–30. doi:10.1103/PhysRevC.55.424
[40] Hemmert TR, Holstein BR, Knochlein G, Scherer S. Virtual Compton scattering off the nucleon in chiral perturbation theory. Phys Rev (1997) D55:2630–43. doi:10. 1103/PhysRevD.55.2630
[41] Hemmert TR, Holstein BR, Knochlein G, Scherer S. Generalized polarizabilities and the chiral structure of the nucleon. Phys Rev Lett (1997) 79:22–5. doi:10.1103/ PhysRevLett.79.22
[42] Kao C-W, Vanderhaeghen M. Generalized spin polarizabilities of the nucleon in heavy baryon chiral perturbation theory at next-to-leading order. Phys Rev Lett (2002) 89:272002. doi:10.1103/PhysRevLett.89.272002
[43] Kao C-W, Pasquini B, Vanderhaeghen M. New predictions for generalized spin polarizabilities from heavy baryon chiral perturbation theory. Phys.Rev. (2004) D70: 114004. doi:10.1103/PhysRevD.70.114004
[44] Hemmert TR, Holstein BR, Knochlein G, Drechsel D. Generalized polarizabilities of the nucleon in chiral effective theories. Phys Rev (2000) D62:014013. doi:10.1103/ PhysRevD.62.014013
[45] Pascalutsa V, Phillips DR. Effective theory of the Delta(1232) in Compton scattering off the nucleon. Phys Rev (2003) C67:055202. doi:10.1103/PhysRevC.67. 055202
[46] Lensky V, Pascalutsa V, Vanderhaeghen M. Generalized polarizabilities of the nucleon in baryon chiral perturbation theory. Eur Phys J (2017) C77:119. doi:10.1140/ epjc/s10052-017-4652-9
[47] Roche J, Friedrich JM, Lhuillier D, Bartsch P, Baumann D, Berthot J, et al. First determination of generalized polarizabilities of the proton by a virtual compton scattering experiment. Phys Rev Lett (2000) 85:708–11. doi:10.1103/PhysRevLett.85.708
[48] d'Hose N. Virtual compton scattering at MAMI. Eur Phys J (2006) A28S1:117–27. doi:10.1140/epja/i2006-09-013-6
[49] Laveissiere G, Todor L, Degrande N, Jaminion S, Jutier C, Di Salvo R, et al. Measurement of the generalized polarizabilities of the proton in virtual Compton scattering at Q2 = 0.92 GeV2 and 1.76 GeV2. Phys Rev Lett (2004) 93:122001. doi:10. 1103/PhysRevLett.93.122001
[50] Fonvieille H, Laveissière G, Degrande N, Jaminion S, Jutier C, Todor L, et al. Virtual compton scattering and the generalized polarizabilities of the proton at Q2 = 0.92 and 1.76 GeV2. Phys.Rev. (2012) C86:015210. doi:10.1103/PhysRevC.86.015210
[51] Bourgeois P, Sato Y, Shaw J, Alarcon R, Bernstein AM, Bertozzi W, et al. Measurements of the generalized electric and magnetic polarizabilities of the proton at low Q2 using the VCS reaction. Phys Rev Lett (2006) 97:212001. doi:10.1103/ PhysRevLett.97.212001
[52] Bourgeois P, Sato Y, Shaw J, Alarcon R, Bernstein AM, Bertozzi W, et al. Measurements of the generalized electric

and magnetic polarizabilities of the proton at low Q2 using the virtual Compton scattering reaction. Phys Rev (2011) C84:035206. doi:10.1103/PhysRevC.84.035206
[53] Janssens P, Doria L, Achenbach P, Ayerbe Gayoso C, Baumann D, Bernauer JC, et al. A New measurement of the structure functions PLL PTT/ and PLT in virtual Compton scattering at Q2 = 0.33 (GeV/c)2. Eur Phys J (2008) A37:1–8. doi:10.1140/epja/ i2008-10609-3
[54] Blomberg A, Atac H, Sparveris N, Paolone M, Achenbach P, Benali M, et al. Virtual Compton Scattering measurements in the nucleon resonance region. Eur Phys J (2019) A55:182. doi:10.1140/epja/i2019-12877-0
[55] Beričič J, Correa L, Benali M, Achenbach P, Ayerbe Gayoso C, Bernauer J, et al. New insight in the Q2-dependence of proton generalized polarizabilities. Phys Rev Lett (2019) 123:192302. doi:10.1103/PhysRevLett.123.192302
[56] Virtual compton scattering on the proton. In New avenues in lepton scattering,846 Parallel Workshop (EINN 2017 Conference)
[57] Li R, Sparveris N, Atac H, Jones MK, Paolone M, Akbar Z, et al. Measured proton electromagnetic structure deviates from theoretical predictions. Nature (2022) 611: 265–70. doi:10.1038/s41586-022-05248-1
[58] Measurement of the Generalized Polarizabilities of the Proton in Virtual Compton Scattering, JLab Experiment E12-23-001.
[59] Gorchtein M, Lorce C, Pasquini B, Vanderhaeghen M. Light-front interpretation of proton generalized polarizabilities. Phys Rev Lett (2010) 104:112001. doi:10.1103/ PhysRevLett.104.112001
[60] Tiesinga E, Mohr PJ, Newell DB, Taylor BN. CODATA recommended values of the fundamental physical constants: 2018. RevMod Phys (2021) 93:025010. doi:10.1103/ RevModPhys.93.025010
[61] H. Fonvieille, B. Pasquini, N. Sparveris, Prog. Part. Nucl. Phys. 113, 103754 (2020)
[62] R. Li, et al., Nature 611, 265 (2022)
[63] P.A.M. Guichon, G.Q. Liu and A.W. Thomas, Nucl. Phys. A 591 (1995) 606.
[64] D. Drechsel, G. Knochlein, A.Y. Korchin, A. Metz, S. Scherer, Phys. Rev. C 57, 941 (1998)
[65] D. Drechsel, G. Knochlein, A.Y. Korchin, A. Metz, S. Scherer, Phys. Rev. C 58, 1751 (1998)
[66] V. Olmos de Leon, et al., Eur. Phys. J. A10 (2001) 207
[67] Pasquini, B. and Vanderhaeghen, M. Dispersion Theory in Electromagnetic Interactions Annu. Rev. Nucl. Part. Sci. 68, 75-103 (2018).
[68] B. Pasquini, M. Gorchtein, D. Drechsel, A. Metz, M. Vanderhaeghen, Eur. Phys. J. A11 (2001) 185-208.
[69] D. Drechsel, B. Pasquini, M. Vanderhaeghen, Phys. Rept. 378 (2003) 99-205.
[70] D. Drechsel, O. Hanstein, S.S. Kamalov, L. Tiator, Nucl. Phys. A 645, 145 (1999)
[71] J. Roche, et al., Phys. Rev. Lett. 85 (2000) 708-711.
[72] P. Janssens, et al., Eur. Phys. J. A37 (2008) 1-8
[73] G. Laveissiere, et al., Phys. Rev. Lett. 93 (2004) 122001
[74] H. Fonvieille, et al., Phys. Rev. C86 (2012) 015210
[75] P. Bourgeois, et al., Phys. Rev. Lett. 97 (2006) 212001
[76] P. Bourgeois, et al., Phys. Rev. C 84 (2011) 035206
[77] MAMI experiment A1/1-09, H. Fonvieille et al, *A study of the Q^2-dependence of the structure functions $P_{LL} - P_{TT}/\epsilon$ and P_{LT} and the generalized polarizabilities α_E and β_M in Virtual Compton Scattering at MAMI.*
[78] MAMI experiment A1/3-12, N. Sparveris et al, *Study of the nucleon structure by Virtual Compton Scattering measurements at the Δ resonance.*
[79] V. Bernard, N. Kaiser, A. Schmidt, U.G. Meissner, Phys. Lett. B 319, 269 (1993) and references therein
[80] T. R. Hemmert, B. R. Holstein, G. Knochlein, S. Scherer, Phys. Rev. D55 (1997) 2630-2643.
[81] T. R. Hemmert, B. R. Holstein, G. Knochlein, S. Scherer, Phys. Rev. Lett. 79 (1997) 22-25.
[82] T. R. Hemmert, B. R. Holstein, G. Knochlein, D. Drechsel, Phys. Rev. D62 (2000) 014013.
[83] C. W. Kao, M. Vanderhaeghen, Phys. Rev. Lett. 89 (2002) 272002.
[84] C.-W. Kao, B. Pasquini, M. Vanderhaeghen, Phys. Rev. D70 (2004) 114004.
[85] G. Q. Liu, A. W. Thomas, P. A. M. Guichon, Austral. J. Phys. 49 (1996) 905-918.
[86] B. Pasquini, S. Scherer, D. Drechsel, Phys. Rev. C63 (2001) 025205.
[87] B. Pasquini, G. Salme, Phys. Rev. C57 (1998) 2589.
[88] A. Metz, D. Drechsel, Z. Phys. A356 (1996) 351-357.
[89] A. Metz, D. Drechsel, Z. Phys. A359 (1997) 165-172.
[90] M. Vanderhaeghen, Phys. Lett. B368 (1996) 13-19.
[91] M. Kim, D.-P. Min (1997) [hep-ph/9704381]
[92] W. Detmold, B. Tiburzi, A. Walker-Loud, Phys. Rev. D 81, 054502 (2010)
[93] A.I. Lvov, S. Scherer, B. Pasquini, C. Unkmeir, D. Drechsel, Phys. Rev. C 64, 015203 (2001)
[94] M. Gorchtein, C. Lorc´e, B. Pasquini, M. Vanderhaeghen, Phys. Rev. Lett. 104, 112001 (2010)
[95] B. Pasquini, D. Drechsel, and M. Vanderhaeghen, Eur. Phys. J. Special Topics 198, 269285 (2011)
[96] H. Fonvieille, Talk at "New Vistas in Low-Energy Precision Physics (LEPP)", Mainz, April 2016; `https://indico.mitp.uni-mainz.de/event/66/session/3/contribution/25/material/slides/1.pdf`
[97] N.D.'Hose, Eur. Phys. J. A28, S01 (2006) 117-127
[98] https://www.jlab.org/Hall-C/upgrade/
[99] https://www.jlab.org/Hall-C/equipment/HMS.html
[100] https://hallcweb.jlab.org/wiki/index.php/Monte_Carlo
[101] N. Sparveris et al, Phys. Rev. C 78, 025209 (2008)

[102] J. Bericic, et al., Phys. Rev. Lett. 123 (2019) 192302
[103] H. Fonvieille, et al., Phys. Rev. C 103 (2021) 025205
[104] A. Blomberg, et al., Eur. Phys. J A 55, 182 (2019)
[105] V. Lensky, V. Pascalutsa, and M. Vanderhaeghen, Eur. Phys. J. C77, 119 (2017).
[106] Rasmussen, C. E., and Williams, C. K. I. Gaussian Processes for Machine Learning the MIT Press, Cambridge Massachusetts, 2006, ISBN 026218253X, ©2006 Massachusetts Institute of Technology
[107] X. Li, et al., Phys. Rev. Lett. 128 (2022) 132502
[108] E. Mornacchi e, et al., Phys. Rev. Lett. 128 (2022) 132503
[109] Fonvieille, H., Conference talk, EINN 2017, Cyprus, (http://2017.einnconference.org/wp-content/uploads/2017/11/EINN-2017-Final-Programme.pdf)
[110] H. Fonvieille, Lecture, *Virtual Compton Scattering*, SFB School 2017, Boppard (https://indico.mitp.uni-mainz.de/event/89/)
[111] I.K. Bensafa et al., Eur.Phys.J.A 32 (2007) 69-75
[112] B. Pasquini and M. Vanderhaeghen, Eur. Phys. J. A 57 (2021) 11, 316